Structural Dynamics of Distal Histidine Replaced Mutants of Myoglobin Accompanied with the Photodissociation Reaction of the Ligand†

Masaaki Sakakura,§ Isao Morishima,‡ and Masahide Terazima*,§

Department of Chemistry, Graduate School of Science, Kyoto University, Kyoto 606-8502, Japan, and Department of Molecular Engineering, Graduate School of Engineering, Kyoto University, Kyoto 606-8501, Japan

Received December 21, 2001; Revised Manuscript Received February 18, 2002

ABSTRACT: Protein dynamics observed by the transient grating (TG) method are studied for some site-directed mutants at the distal histidine of myoglobin (H64L, H64Q, H64V). The time profiles of the TG signals are very sensitive to the amino acid residue of the 64 position. It was found that the sensitivity is mostly caused by the different rates of the ligand escape from the protein to solvent and the magnitude of the molecular volume change. Several molecular origins of the volume difference between MbCO and Mb, such as the electrostatic interaction in the distal pocket, movement of helices, and distal water, are proposed. Interestingly, the volume difference between the CO-trapped Mb inside the protein interior and Mb is similar to that of the partial molar volume of CO in organic solvent. The effect of mutation on the nature of the CO trapped site is discussed.

1. INTRODUCTION

The protein dynamics accompanied with the photodissociation of carboxymyoglobin (MbCO) has been a typical target for elucidating the relationship between protein structure dynamics and function for a long time (*1*−*5*), because the protein motion of myoglobin plays very important roles in the ligand dissociation−association process. According to X-ray crystallographic data of deoxyMb, MbCO, and MbO_2, it was suggested that the transient channel formed by protein motion should be essential for the ligand to move between the protein interior and the solvent (*6*−*8*). To detect the protein motion, various spectroscopic methods, such as time-resolved IR (*9*, *10*), CD (*11*), Raman (*12*−*14*), and visible absorption detection (*1*, *15*−*23*), have been used for studying the photodissociation reaction of MbCO. Time-resolved resonance Raman scattering and visible absorption studies have revealed many kinetics of this reaction (*12*−*21*). These signals are rather sensitive only for the local structural change around the chromophore (heme). In this paper, we focus our attention on the dynamics of more global protein structure after the photodissociation of CO for several site-directed mutants at the distal histidine using the time-resolved transient grating (TG) and photoacoustic (PA) techniques.

It has been known that the TG and PA methods are powerful methods to study the global structural changes during chemical reaction by monitoring the volume changes (ΔV) and the enthalpy changes (ΔH) (*24*−*32*). Peters and co-workers studied ΔH and ΔV of the photodissociation reaction of MbCO by the PA method under an assumption that the volume change does not depend on temperature (*31*). They observed a fast (<10 ns; $\Delta H = 3.4$ kJ mol^{-1} and $\Delta V = -9.0$ cm^3 mol^{-1}) and slow (~700 ns at 20 °C; $\Delta H = 42$ kJ mol^{-1} and $\Delta V = 5.1$ cm^3 mol^{-1}) dynamics and interpreted the observed ΔH and ΔV in terms of the salt bridge breaking and reformation. Miller and co-workers investigated the structure change of Mb using the TG technique and observed an anisotropic structural change (*29*). They concluded that the structure change completes within 5 ps after the photoexcitation. We studied ΔH and ΔV in a range of tens of nanoseconds to a few milliseconds by the TG and PA methods quantitatively. We determined ΔH and ΔV without any assumption for the first time and found that the values are different from the previously reported ones by the PA method (*26*, *27*). For example, the volume changes are initially contraction of 5 cm^3 mol^{-1} within 10 ns and expansion of 12 cm^3 mol^{-1} with a lifetime of 700 ns at 20 °C in a case of sperm whale (SW) MbCO (*27*). The enthalpy differences of the first and the second intermediate species from the original species (MbCO) are 70 and 62 kJ mol^{-1}, respectively. We and Dadusc et al. also clearly attributed the 700 ns-dynamics (at 20 °C) to the ligand (CO) escaping process from the protein part (*27*, *28*). Although the global structural dynamics was detected clearly by these studies, the molecular origin of the volume change is less clear.

In the previous study, we interpreted the observed ΔH and ΔV in terms of the movement of the helices and the CO escaping from the protein interior (*26*, *27*). Although they are very plausible origins of ΔH and ΔV, there are several other factors we should examine. One of them is a role of distal water, which is hydrogen bonded to the distal His (His64) in five-coordinate deoxyMb (*2*, *33*, *34*). A water molecule could enter the protein interior after the ligand escapes from the ligand-binding site (*2*, *23*), and this process may change the protein volume. The electrostatic interaction between the bound CO and the distal pocket, which is shown

† A part of this study was supported by the Grant-in-Aid (No. 13853002) from the Ministry of Education, Science, Sports and Culture in Japan and Scientific Research Grants from Mitsubishi Foundation.

* To whom correspondence should be addressed.

§ Department of Chemistry, Graduate School of Science.

‡ Department of Molecular Engineering, Graduate School of Engineering.

10.1021/bi016085d CCC: $22.00
Published on Web 03/22/2002

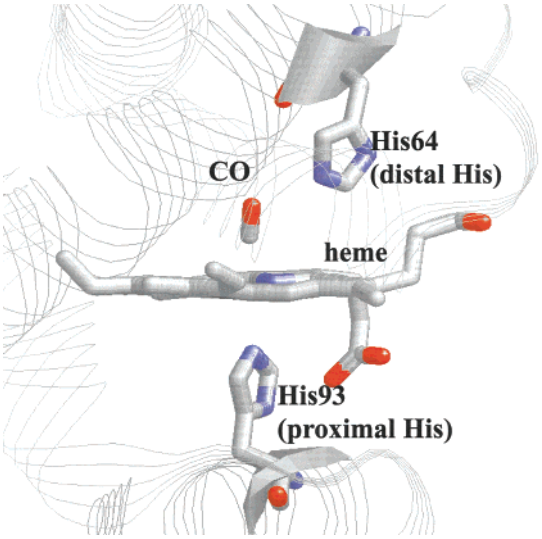

FIGURE 1: The structure around heme of sperm whale MbCO (*32*). CO is bound to heme iron at the distal side of heme. The atomic coodinates were obtained from the protein data bank (PDB).

by previous Raman (*12*, *13*, *35*), IR (*36*), and MD simulation (*37*) studies using the distal pocket polarity dependence of the CO stretching frequency, could be also important to consider the origins of volume change, because the production of free CO after the photodissociation is expected to cause the disappearance of the interaction (*37*) and the global structure change. Peters and co-workers interpreted the volume change in terms of the breaking and forming of the salt bridge between Arg45 and heme propionate side chain (*31*).

Site-directed mutation technique has been utilized with various spectroscopic experiments to help uncover the role of a specific amino acid residue in the overall structural dynamics (*2*, *12*−*14*, *18*, *19*, *22*, *31*, *34*, *36*). To reveal the possible contribution described above, we focused our attention on the role of the distal His (His64; Figure 1), because this residue is associated with distal water (*33*), the electrostatic interaction between CO and the distal pocket (*35*−*37*), the salt bridge, and close-opened form of Mb (*8*, *13*, *31*). The X-ray study by Quillin et al. showed that the distal water, which can be clearly observed in wild-type deoxyMb, is absent in deoxyMb mutants in which His64 is replaced by the other amino acids such as Leu and Gln (*33*). Previous flash photolysis studies suggested that the distal water plays a key role in determining the energy barrier for the ligand binding from the comparison of the recombination kinetics of WT-MbCO with that of His64-replaced MbCO (*2*, *23*). IR and Raman studies (*13*, *35*, *36*) as well as an MD simulation study (*37*) led a conclusion that the electrostatic interaction in the distal pocket of MbCO is very sensitive to the polarity of residue 64. Hence, substitution of distal His with other amino acids and comparison of their structural dynamics should provide clues to consider the origins of volume change related to the above expectation.

In this study, we investigate the structural change of some site-directed mutants of SW-Mb, in which the His64 (distal His) was replaced by Leu (H64L), Val (H64V), and Gln (H64Q). We found that the time profiles of the TG signals are very sensitive to the amino acid at this position, and discussed the role of the His64 of SW-MbCO in the photodissociation process from a point of the volume and the enthalpy changes associated with this reaction.

2. PRINCIPLE

To detect the global structural change and measure ΔH and ΔV after the photoexcitation of MbCO, we used the TG-PA hybrid technique. The method was described in detail previously (*24*−*27*). Here, we briefly summarize the principle of the TG and PA and how to determine ΔH and ΔV.

In the TG method, two coherent laser pulses were crossed in a sample to create the interference pattern of the light intensity. Any photophysical and photochemical process induced by the interference pattern creates spatially modulation of the refractive index and the absorption. These modulations diffract a probe beam in the direction that satisfies the Bragg condition (TG signal). Under the weak diffraction condition, the intensity of the TG signal (I_{TG}) is given by eq *1* (*38*)

$$I_{TG}(t) = \alpha(\delta n(t))^2 + \beta(\delta k(t))^2 \qquad (1)$$

where α and β are constants, and $\delta n(t)$ and $\delta k(t)$ are the peak-null difference of the refractive index and the absorbance, respectively. The time profile of the TG signal represents variety of dynamics such as the energy relaxation, the thermal diffusion, the kinetics of the excited states, chemical reaction, and mass diffusion. Under the present experimental conditions, the refractive index change (δn) consists of two contributions: the thermal grating (δn_{th}) and the species grating (δn_{spe}) (*24*). The thermal grating is caused by the thermal energy due to the nonradiative transition and the enthalpy change of a reaction. When the thermal energy $Q(t)$ is released, the time profile of the thermal grating ($\delta n_{th}(t)$) is given by

$$\delta n_{th}(t) = [(dn/dT)(W/\rho C_p)][(dQ(t)/dt) \otimes \exp(-q^2 D_{th} t)] \qquad (2)$$

where dn/dT is the refractive index change by the temperature variation of the solution, C_p is the heat capacity ($JK^{-1}\,mol^{-1}$), W is the molecular weight (g/mol), ρ is the density (g/cm^3) of the solvent, D_{th} is thermal diffusivity ($m^2\,s^{-1}$), q is the magnitude of the grating vector (m^{-1}) and $\otimes$ denotes the convolution integral. For example, the photodissociation process of MbCO has two steps in thermal energy releasing; the thermal energy of Q_f and Q_s is released within the pulse width and with a time constant of τ_s, respectively. In this case, $\delta n_{th}(t)$ can be written as

$$\delta n_{th}(t) = \left(\frac{dn}{dT}\right)\frac{W}{\rho C_p}\left\{\left[Q_f + Q_s\left(1 - \frac{\tau_s}{\tau_{th}}\right)^{-1}\right]\exp\left(-\frac{t}{\tau_{th}}\right) + Q_s\left(1 - \frac{\tau_s}{\tau_{th}}\right)^{-1}\exp\left(-\frac{t}{\tau_s}\right)\right\} \qquad (3)$$

The species grating (δn_{spe}) is created by the refractive index change due to the creation or depletion of chemical species. If the concentration of the chemical species are constant during the observation time, the time profile of the species grating (δn_{spe}) is given by ref *24*

$$\delta n_{spe}(t) = \sum_i \delta n^i_{spe} \exp(-D_i q^2 t) \qquad (4)$$

where D_i is the diffusion coefficients of the species i and δn^i_{spe} is the refractive index change due to the presence of the species i. In the species grating term, there are two contributions: one comes from absorption change (the population grating δn_{pop}), and the other is due to the molecular volume change (the volume grating δn_V).

To determine ΔV of the reaction, we sometimes used the photoacoustic (PA) method, which detects a pressure wave created by the thermal expansion and molecular volume change. When the time profiles of the volume change and thermal releasing are written by $\Delta V(t)$ ($cm^3\ mol^{-1}$) and $Q(t)$ (J/mol), the intensity of the PA signal can be written as follows (*24*−*27*, *31*):

$$I_{PAS}(t) = A'\left(d\Delta V(t)/dt + \frac{(d\Delta Q(t)/dt)W}{\rho C_p}\alpha_{th}\right) \otimes g(t) \quad (5)$$

where A' is a proportional constant, which is determined by both the sensitivity of the apparatus and the experimental condition, $g(t)$ is an instrument response function, and α_{th} is the thermal expansion coefficient. Once we determine the thermal energy by the TG method, we can determine the volume change by subtracting the thermal contribution from the PA signal.

3. EXPERIMENTAL SECTION

Setup for TG and PA Experiment. In the TG measurement, a laser beam from the second harmonics of a Nd:YAG laser (Spectra Physics, GCR170; $\lambda = 532$ nm; pulse width ~ 10 ns) was split into two with a beam splitter and crossed in the sample by a lens (focus length = 20 cm) to create the transient grating. The transient grating was detected as a diffraction of a CW probe beam (diode laser; SDL-5411-G1, 840 nm) that was lead into the transient grating region with the angle satisfying a Bragg condition. The diffracted beam (TG signal) was detected by a photomultiplier after passing a pinhole (*24*−*27*). For a high wavenumber TG experiment, the two excitation beams were focused by separated lenses (focus length = 20 cm) to achieve a large crossing angle ($\sim$50°) (*39*).

For the PA experiment, the pressure wave produced by photoexcitation of the sample by the second harmonics of the Nd:YAG laser was detected by a piezoelectric transducer (PZT) (*24*, *26*, *27*). The TG and PA signals were averaged by a digital oscilloscope (Tektronix TDS-520 or Tektronix 2430A) and a microcomputer. Both for the TG and PA experiments, malachite green (*40*) solved in distilled water was used as a calorimetric reference.

To control the temperature of the sample, the sample cell was placed in the metal cell holder, and the methanol was circulated around the cell holder by a thermostated bath (Lauda RLS6-D). The temperature of the sample was monitored by a thermocouple wire and a digital voltmeter.

Sample Preparation. Site-directed mutagenesis of recombinant Mb at the position of 64 was carried out by the polymerase chain reaction (PCR) based technique with pUC vector containing the sperm whale Mb gene as a template. The wild type and mutant Mbs (H64L, H64V, and H64Q) were expressed by *Escherichia coli* strain TB I and purified by the same method as reported (*41*). By adding 10 mM Tris-HCl buffer, the final sample concentration was adjusted to nearly 0.4 mM. For preparation for MbCO, met Mb solution in 10 mM Tris-HCl buffer was filtered to remove small particles by a membrane filter, and was sealed in a 2 mm path length quartz cell with a rubber septum. Mb was reduced by sodium dithionite after passing N_2 for 30 min through the sample cell, and CO was passed over for 1 h to yield the CO form. The spectrum of the sample was checked before and after the experiment by the UV−visible spectrometer (Shimazu UV-2500 PC) to confirm that MbCO did not convert to other compound.

4. RESULTS

In this paper, we study the volume and enthalpy changes after the photodissociation reaction of CO from the heme for the site-directed mutants at the residue 64. Although the TG signal of the wild type (WT) SW-MbCO was described and analyzed in detail in the previous paper (*27*), we first briefly summarize the features here for a comparison purpose with the TG signal of the mutants.

4.1. WT SW-MbCO. Figure 2 a shows the TG signal of SW-MbCO in 10 mM Tris buffer at 20 °C. The signal rises within a pulse width and is followed by two decay-rise components. The first decay-rise component has a lifetime of 700 ns at 20 °C. The decay-rise feature comes from the destructive interference between the 700 ns component and components with much longer lifetimes. The signal intensity at the bottom of the interference dip represents the amplitude of the grating due to the absorption change (δk). We have attributed the 700 ns kinetics to a volume change as well as a heat releasing process. The following decay-rise component from 10^{-6} s to 2×10^{-5} s was attributed to the destructive interference between the thermal grating (δn_{th}) and the species grating (δn_{spe}). The time constant of this kinetics is determined by $D_{th}q^2$. The destructive interference indicates that the signs of δn_{th} and δn_{spe} are opposite. The slowest decay component in submillisecond time scale can be expressed by a biexponential function; the faster component was attributed to the diffusion of the photodissociated CO, and the slower one was assigned to the diffusion of Mb and the recombination process of CO to Mb. The decay rate is about the same as the recombination rate (k_{rec}) observed in a transient absorption because $D_{Mb}q^2$ (D_{Mb}: the diffusion constant of Mb) is much smaller than k_{rec} under this condition. The TG signal in this whole range was fitted by the following equation:

$$I_{TG}(t) = \alpha[\delta n_s \exp(-k_s t) + \delta n_{th} \exp(-D_{th}q^2 t) + \delta n_{CO} \exp(-D_{CO}q^2 t) + \delta n_{Mb} \exp(-k_{rec} t)]^2 + \beta(\delta k_{spe} \exp(-k_{rec} t))^2 \quad (6)$$

where δn_s, δn_{th}, δn_{CO}, and δn_{Mb} are the refractive index changes due to the 700 ns kinetics, heat releasing, CO, and Mb, respectively, and δk_{spe} is the absorption change. In summary, two kinetics of volume and enthalpy changes can be observed in the TG signal of WT-MbCO; the faster ones, which occur within a pulse width, are denoted by ΔH_f and ΔV_f, and the slower ones with a lifetime of several hundred nanoseconds are denoted by ΔH_s and ΔV_s, respectively.

From the amplitude of δn_{th}, the released thermal energy was determined to be 159 ($\pm$ 20) kJ mol^{-1}. Since the quantum yield for the photodissociation of WT-MbCO is

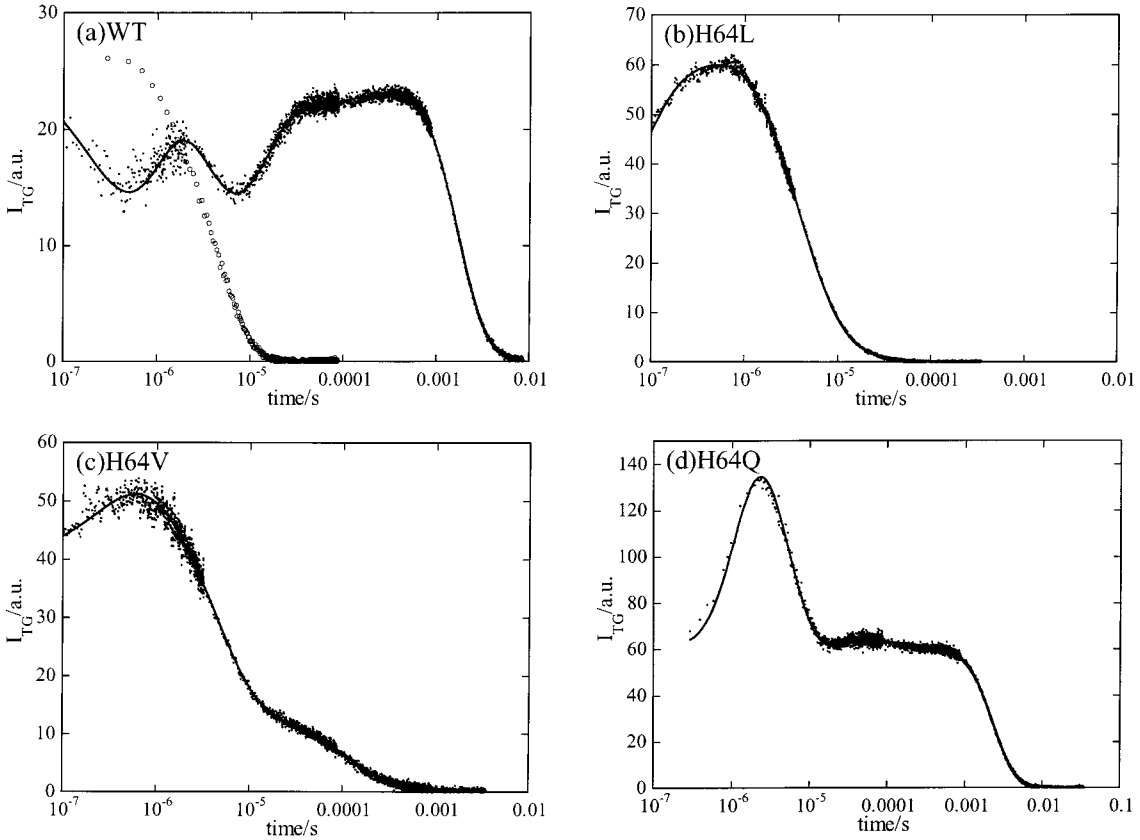

FIGURE 2: The dotted lines represent the observed TG signals after the photodissociation of (a) WT, (b) H64L, (c) H64V, and (d) H64Q sperm whale MbCO in 10 mM Tris buffer (pH = 7) at ambient temperature. The grating wavenumbers of the signals are (a) $q = 9.7 \times 10^5$ m^{-1}, (b) 10.3×10^5 m^{-1}, (c) 9.11×10^5 m^{-1}, and (d) 8.66×10^5 m^{-1}. The best fitted signals are represented by solid lines. The decaying signal represented by open circles in panel a is the TG signal of malachite green (MG) in aqueous solution measured under the same condition.

0.96 (*17*), the enthalpy change during the process of MbCO → Mb+CO should be $\Delta H = 70$ (± 20) kJ mol^{-1}. The analysis of the 700 ns dynamics at 20 °C has shown that the volume change and enthalpy change during this process are $\Delta V_s = 12$ (± 1) kJ mol^{-1} and $\Delta H_s = 8$ (± 5) kJ mol^{-1}, respectively.

From the PA measurement (Figure 3 a), the volume change during the process of MbCO → Mb+CO was determined to be $\Delta V_{total} = 7$ (± 3) cm^3 mol^{-1}. Therefore, the volume change within a pulse width was determined to be $\Delta V_f = -5$ (± 3) cm^3 mol^{-1}.

4.2. H64L. The photodissociation process of H64L-MbCO was studied by Carver et al. using the transient absorption (TA) method (*18*). According to their study, the quantum yield of the geminate recombination of H64L-MbCO is 39% and the geminate recombination kinetics is expressed by a biexponential function with lifetimes of 50 ns (28% amplitude in the total signal intensity) and 420 ns (11%) at 20 °C. This biphase dynamics was explained by the four-state model of the dissociation. The rate of the bimolecular rebinding of CO to Mb is much faster than that of WT-MbCO. The data are used for the analysis of the TG signal.

Figure 2b depicts the TG signal of H64L in 10 mM Tris buffer at 20 °C. Initially, the signal rises with a system response time constant, followed by a slow rising component with 50 and 400 ns lifetimes. The intensity of this slow rising component is much smaller than that of WT-MbCO. The signal decays to the baseline with roughly a biexponential function. Since the faster decay rate constant agrees well with $D_{th}q^2$ under this experimental condition, this component is reasonably attributed to the thermal grating. The slower decay rate is close to the decay rate of the TA signal and the rate depends on the CO concentration. Hence, this dynamics represents the bimolecular recombination process of H64L-Mb and CO. This rate is about 50 times faster than that of WT-MbCO, and it agrees well with the value reported previously (*18*).

It should be noted that the thermal grating component (δn_{th}) and the species grating component (δn_{spe}) of H64L-MbCO is constructively interfered, whereas the interference between these components for WT-MbCO was destructive as described in the previous section. This constructive interference means that the sign of δn_{spe} is negative (i.e., same as that of δn_{th}) for H64L. As described in the principle section, there are two contributions in δn_{spe}; population and volume gratings. The sign of the population grating is expected to be positive from the absorption spectra of MbCO and Mb (*26*, *27*). Indeed, δn_{spe} of WT-MbCO is positive because of this contribution. Therefore, the negative δn_{spe} for this mutant should be due to the large negative contribution of the volume term; that is, the molecular volume change just after the photodissociation is the volume expansion instead of volume contraction for WT-MbCO, because volume expansion induces negative refractive index change (δn_V). If we assume that δn_{pop} of H64L is the same as that of WT-MbCO, molecular volume change is calculated to be 22 cm^3 mol^{-1}. This value agrees quite well with that

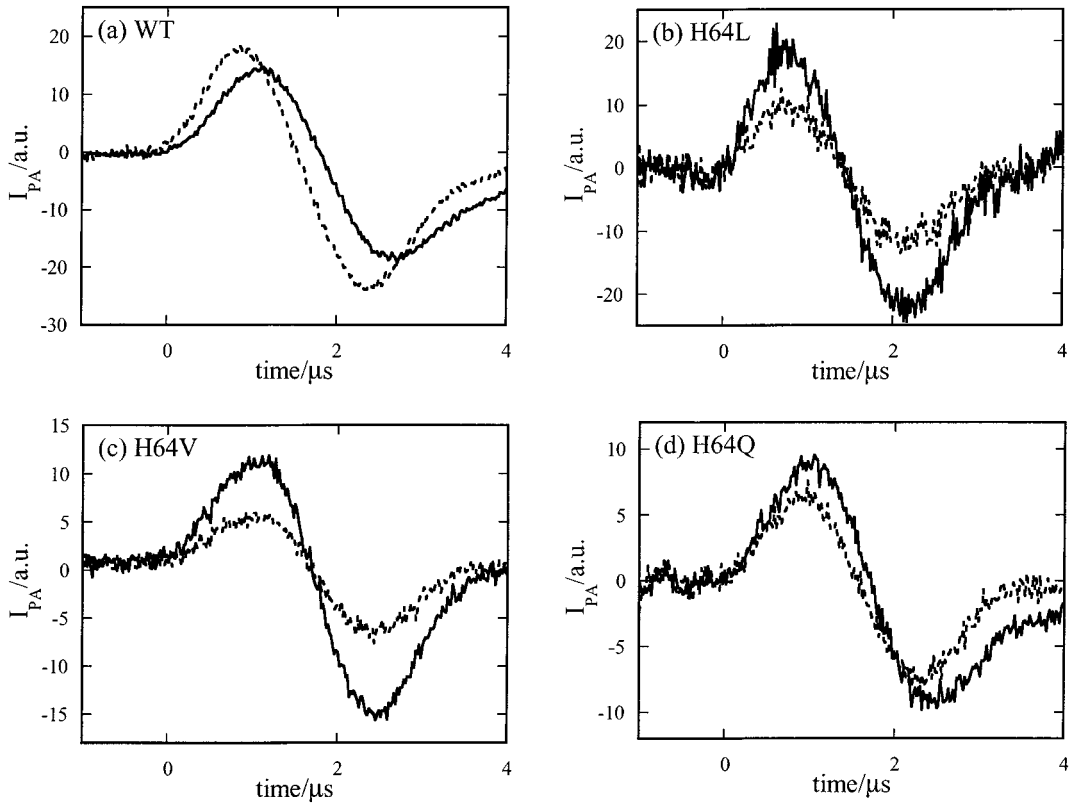

FIGURE 3: The PA signals of (a) WT, (b) H64L, (c) H64V, and (d) H64Q sperm whale MbCO in buffer at ambient temperature (solid line). The dotted line in each figure is the PA signal of reference (MG in aqueous solution) under the same condition.

measured by using the PA method independently as described later in this section.

The observed signal in the whole observation range can be reproduced well by eq 7

$$I_{TG}(t) = \alpha\Big[\delta n_{s1}\exp\Big(-\frac{t}{50\text{ ns}}\Big) + \delta n_{s2}\exp\Big(-\frac{t}{420\text{ ns}}\Big) + \delta n_{th}\exp(-D_{th}q^2t) + \delta n_{spe}\exp(-k_{rec}t)\Big]^2 + \beta\Big[\frac{1}{0.61}\delta k_{spe}\Big(0.28\exp\Big(-\frac{t}{50\text{ ns}}\Big) + 0.11\exp\Big(-\frac{t}{420\text{ ns}}\Big) + 0.61\exp(-k_{rec}t)\Big)\Big]^2 \quad (7)$$

Here some of the lifetimes (50 ns, 420 ns, $D_{th}q^2$, and k_{rec}) were fixed during the least-squares fitting of the TG signal to reduce the number of adjustable parameters and to avoid the fitting ambiguity. These rates we used were determined independently from the geminate recombination kinetics measured by the TA method (50 ns, 420 ns, and k_{rec}) (*18*) and from the decay rate of the thermal grating signal of the calorimetric reference sample ($D_{th}q^2$). The preexponential factors for the amplitude grating components were also fixed in the same way. From this fitting, the ratio of the refractive index changes for the two slow rising was found to be δn_{s1}: δn_{s2} = 28:11. This ratio is the same as the ratio of the amplitude grating and the TA signal. This fact indicates that the refractive index change of this component is mainly determined by the population grating component and, therefore, volume changes during the 50 and 420 ns dynamics are negligible.

Comparing the thermal grating intensities of H64L with that of MG (calorimetric reference), we found that the thermal energy of 191 kJ mol^{-1} is released by the photodissociation. Since the quantum yield of the dissociation is 0.61 (*18*), the enthalpy difference between MbCO and Mb+CO for H64L is ΔH = 61 (± 17) kJ mol^{-1}.

The PA signal of H64L in the buffer and MG in water at 22 °C under the same conditions are shown in Figure 3b. We could not observe any temporal shift of the PA signal of H64L compared with the calorimetric reference sample. This fact implies that the acoustic wave from the sample is generated immediately after the photoexcitation. Therefore, the PA signal intensity of H64L directly reflects the thermal expansion and the molecular expansion accompanied with the dissociation reaction. From the comparison of the PA signal for H64L-MbCO with that of MG, it was found that the amplitude of the PA signal for MbCO corresponds to volume expansion of 24.5 cm^3 mol^{-1} at 22 °C. Subtracting the thermal volume expansion contribution of 191 kJ mol^{-1} determined by the TG measurement, one obtains the molecular volume contribution of 14.3 cm^3 mol^{-1}. By using the quantum yield of the photodissociation (ϕ = 0.61) (*18*), the volume expansion from MbCO to Mb+CO for H64L was determined to be 23.4 cm^3 mol^{-1}. It should be noted that this expansion takes place within 20 ns after the photoexcitation.

The volume and the enthalpy changes for H64L are summarized in Table 1.

4.3. H64V. The TA signal from 20 ns to a few milliseconds after the photoexcitation of H64V is almost perfectly expressed by a single-exponential function with a lifetime around 200 ms, which depends on the CO concentration of the solution (*19*, *42*). The absence of the geminate recombination kinetics in the signal indicates that almost all of

Table 1: Enthalpies (ΔH/ kJ mol^{-1}) and Volume Changes (ΔV/ cm^3 mol^{-1}) of the Photodissociation of CO from Wild Type and Three Mutants MbCOs[a]

	wild type	H64L	H64V	H64Q
ΔH_f (kJ mol^{-1})	78 (± 20)	61	~72 (± 20)	~55
ΔH (kJ mol^{-1})	70 (± 20)	61 (± 17)	72 (± 20)	55 (± 10)
ΔV_f (cm^3 mol^{-1})	−5 (± 3)	23.4 (± 1.2)	>17.4 (± 1.2)	3
ΔV_s (cm^3 mol^{-1})	12 (± 1)	~0	<2.2	9.5
τ_s (ns) at 20 °C	700	420	361 (± 20)	850 (± 10)

[a] ΔH_f and ΔH denote the enthalpy difference between MbCO and intermediate and the final state (Mb+CO), respectively. H_f for H64L and H64Q cannot be determined accurately because of the signal to noise.

the photodissociatied CO escape to the solvent. This inefficient geminate recombination should be due to a very slow geminate recombination or due to a fast CO escaping rate from the heme pocket. The overall bimolecular recombination rate is about three times faster than that of WT-MbCO (*19*, *42*).

The TG signals of H64V in the buffer at 21.5 °C are shown in Figure 2c. The signal rises initially very fast and then slowly with two lifetimes of 50 and 360 ns. This feature is similar to that of H64L. The signal decays to the baseline continuously. This decay profile was reproduced well by three exponential functions. Since the faster decay rate constant agrees well with $D_{th}q^2$ under the present experimental conditions, this component is due to the thermal grating. In contrast to H64L, the fitting of the slower decay profile after the thermal diffusion requires two exponential functions. We found that the faster decay rate agrees well with $D_{CO}q^2$. The slower decay rate is close to the decay rate of the TA signal, and the rate depends on the CO concentration. Hence, the faster dynamics represents the molecular diffusion of CO, and the slower dynamics must represent the bimolecular recombination of Mb and CO. The TG signal should be reproduced by

$$I_{TG}(t) = \alpha \times (\delta n_{s1} \exp(-k_{s1}t) + \delta n_{s2} \exp(-k_{s2}t) + \delta n_{th} \exp(-D_{th}q^2t) + \delta n_1 \exp(-D_{CO}q^2t) + \delta n_{spe2} \exp(-k_{rec}t))^2 + \beta(\delta k_{spe} \exp(-k_{rec}t))^2 \quad (8)$$

From the amplitude of the thermal grating signal, the released thermal energy is determined to be 155 (± 20) kJ mol^{-1}. Using the quantum yield of dissociation after the photoexitation (1.0) (*19*, *42*), one obtains the enthalpy difference between MbCO and Mb+CO of H64V to be ΔH = 72 (± 20) kJ mol^{-1}. Since no slow rising component is observed in the TA signal, the slower rise process with 360 ns observed in the TG signal should be spectrally silent dynamics and must come from the thermal energy releasing or the volume change. The amplitude of this component is much smaller than that of WT-MbCO, and it corresponds to the volume expansion of 2.2 cm^3 mol^{-1}.

The PA signals of H64V-MbCO in the buffer and of MG in water at 23.5 °C are shown in Figure 3c. ΔV for H64V-MbCO was determined by the same procedure as that for H64L. The amplitudes of the PA signals for H64V-MbCO and MG are plotted against the excitation laser power. From the ratio of the slopes, the PA signal of H64V-MbCO was found to correspond to a volume expansion of 28.5 cm^3 mol^{-1} at 23.5 °C. Considering that the thermal energy of 155 kJ mol^{-1} is released, the molecular volume contribution is 19.6 cm^3 mol^{-1}. Using ϕ = 1.0 for H64V-MbCO (*19*, *42*), the volume change after the photodissociation of H64V-MbCO was determined to be ΔV = 19.6 (± 1.2) cm^3 mol^{-1}.

The volume and the enthalpy changes for H64V are summarized in Table 1.

4.4. H64Q. The kinetics monitored by the transient absorption method of H64Q-MbCO is very similar to that of WT-MbCO. The geminate rebinding rate is about 200 ns, and the rate of the bimolecular recombination is about twice faster than that of WT (*19*).

The TG signal of H64Q shown in Figure 2d is also very similar to that of WT-MbCO. Therefore, it can be fitted by eq 6. The initial slow rising component with a time constant of about 850 ns represents the molecular volume change and the heat releasing. The amplitude of this component corresponds to 9.5 cm^3 mol^{-1}, which is almost same as that of WT.

The PA signal of H64Q is shown in Figure 3d. The PA amplitude is larger than that of the reference sample, which indicates that the volume change of H64Q-MbCO is larger than that of WT. From the amplitude and the enthalpy change determined by the TG signal, the total volume change after the photodissociation of H64Q-MbCO is 12.5 cm^3 mol^{-1}. Since the volume change with the time constant of 850 ns is 9.5 cm^3 mol^{-1}, the volume change within the pulse width was determined to be 3 cm^3 mol^{-1}.

5. DISCUSSION

5.1. Volume Change after the Ligand Escape. In this study, we found that the time profiles of the TG signals strongly depend on the amino acid residue at the position 64. This dependence mainly comes from the different rates of submicrosecond kinetics and the magnitude of the volume changes. The photodissociation of CO from the heme occurs within the excitation pulse (*15*, *16*). Previously, we have shown that the sub-microsecond kinetics represents the ligand escape process from the protein interior to the solvent. Hence, the species just after the excitation laser pulse is an intermediate species (Mb:CO), in which the CO is still inside the protein. The volume change of the faster process (ΔV_f) represents this volume difference between the initial MbCO and the intermediate state Mb:CO. As shown in Figure 4, ΔV_f is negative for WT (−5 cm^3 mol^{-1}) and small positive for H64Q (+3 cm^3 mol^{-1}), whereas ΔV_f for H64L and H64V is largely positive of about 20 cm^3 mol^{-1}. The volume change associated with the ligand escape process (Mb:CO → Mb+CO) is large volume expansion of about 10 cm^3 mol^{-1} for WT and H64Q, and very small for H64L and H64V. The total volume changes defined by $\Delta V_{tot} = V(\text{Mb}) + V(\text{CO}) - V(\text{MbCO})$ (V(MbCO), V(Mb), and V(CO): partial molar volumes of MbCO, Mb, and CO, respectively) are 7, 12.5, 23.4, and 19.6 cm^3 mol^{-1} for WT, H64Q, H64L, and H64V, respectively.

First, we discuss the molecular origins of the volume changes of the myoglobin part after the ligand escape ($\Delta V_{Mb} = V(\text{Mb}) - V(\text{MbCO})$). Here we subtracted the contribution of V(CO) because the partial molar volume of CO is naturally independent of the protein structure. ΔV_{Mb} are calculated from the measured ΔV_{tot} and the partial molar volume of CO (V(CO) = 35 cm^3 mol^{-1} (*25*)), and they are summarized

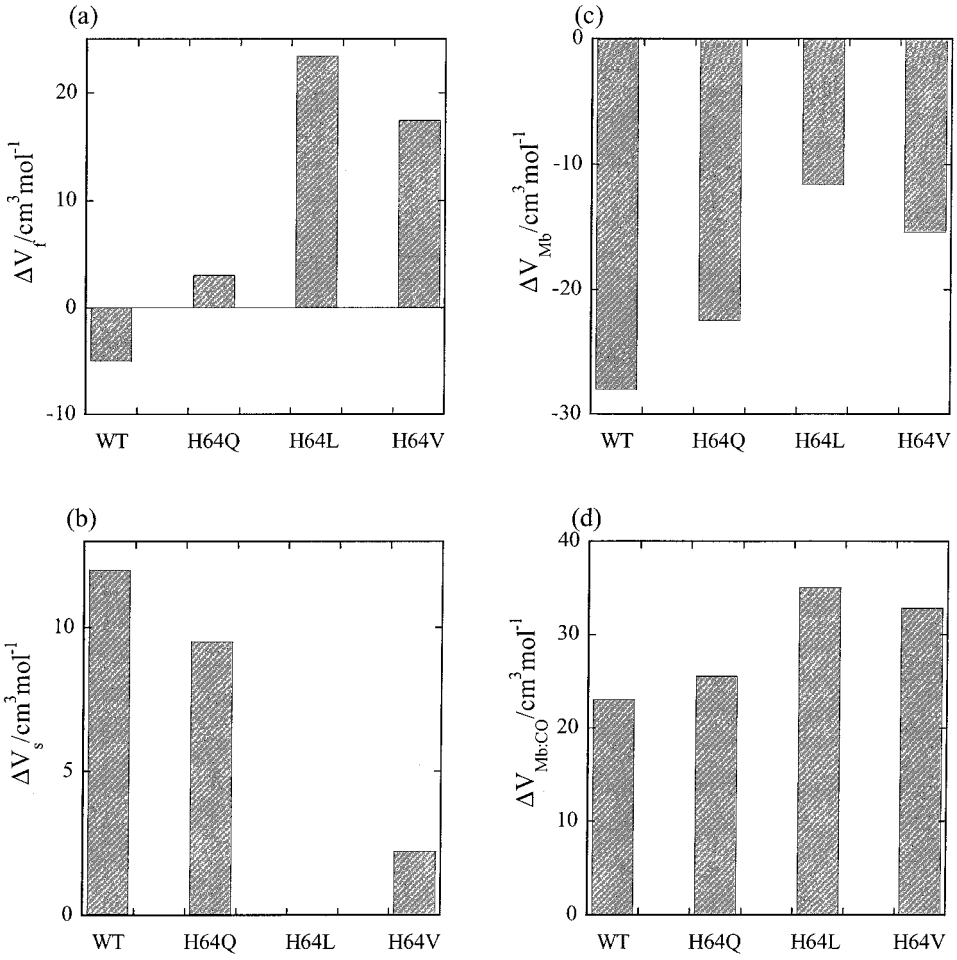

FIGURE 4: Volume changes (ΔV) after the photodissociation of four MbCOs, which were determined by TG-PA hybrid method. (a) ΔV immediately after the photoexcitation of MbCO (ΔV_f), (b) ΔV accompanied with sub-microsecond dynamics (ΔV_s), (c) $\Delta V_{Mb} = V(Mb) - V(MbCO)$, and (d) $\Delta V_{Mb:CO} = V(Mb:CO) - V(Mb)$. $V(Mb)$, $V(MbCO)$, and $V(Mb:CO)$ represent the partial molar volume of Mb, MbCO, and Mb:CO, respectively.

in Figure 4c. In our previous papers (*26*, *27*), we suggested that the volume change after the photodissociation may result from the heme doming process and the following movement of the E and F helices (*43*). However, it is difficult to explain the observed mutant dependence of the volume change only by this contribution. We consider other possible origins of this volume change.

A number of resonance Raman and IR studies showed that the frequencies of CO and CO−Fe stretching bands of MbCO are strongly dependent on pH and the environment of the distal pocket (*12*, *13*, *35*, *36*). Initially, the dependence of the frequencies was attributed to the steric hindrance by the residues 64 and 68, which are located near the bound CO. Later, from the experimental data using various model hemes and mutant Mb, it was concluded that the polarity of the distal pocket is a main factor in determining the frequencies; the CO frequency ν_{CO} is correlated with the polarity and hydrophobicity of the residue 64 (*12*, *13*, *35*, *36*). For example, ν_{CO} of WT (His64) and H64Q, which have polar residue at the position of 64, is observed in 1941 and 1945 cm^{-1}, respectively, whereas H64L and H64V of nonpolar residue 64 have higher ν_{CO} around 1966 cm^{-1} (*12*, *13*, *35*, *36*). Ray et al. explained the correlation between ν_{CO} and the polarity of residue 64 in terms of the electrostatic interaction between the bound CO and the residue 64 (*35*). Their explanation is consistent with the MD simulation by Jawsbury et al., in which they showed that there is a repulsive interaction between the bound CO and polar residue 64 (His64 and Gln64) but no interaction in H64L (*37*). This electrostatic interaction is expected to cause the structural change after the photodissociation. In fact, Quillin et al. have reported that the binding of CO to the heme iron induces significant movements of the residues in the distal pocket from the high-resolution crystal structures (*33*). Dissociation of the CO from the heme pocket decreases the pocket volume of WT and H64Q. In contrast, there are almost no changes in the distal pocket of H64L upon CO binding (Figure 3 in ref *33*). (In their report, they attributed the origin of this difference to the steric repulsion due to His64 and Gln64, but it is now accepted that this repulsion comes from the electrostatic interaction (*37*).) Considering these results, we speculate that the interaction between the bound CO and the residue 64 could be the origin of the mutant dependent volume change of V_{Mb}. Before the photodissociation of CO, the space of the distal pocket is larger for WT and H64Q than for H64L and H64V, because of this repulsive electrostatic interaction. Since larger volume for WT- and H64Q-MbCOs comes from the bound CO, the contraction of the distal pocket space should occur after the photodissociation. This contraction is compensated by the volume expansion caused by the heme doming and E and F helices movement, which should contribute to WT as well as the other mutants.

Another dynamic related with this structural change is the salt bridge breaking. It was suggested that His64 swings out from the protein interior to the solvent and disrupts the salt bridge between Arg45 and the heme 6-propionate side chain to form a channel before the CO escape process (*18*, *44*). A time-resolved Raman scattering spectrum suggests that the salt bridges of H64L- and WT-MbCO are disrupted quickly (<10 and 20 ns, respectively) after the photodissociation and persists until the CO recombination (*13*). This salt bridge is observed for WT and H64Q (*33*), while those for H64L and H64V are not clear. This salt bridge breaking could explain the different volume change between the groups of (WT and H64Q) and (H64L and H64V). However, we have previously shown that ΔV_{Mb} of SW-MbCO is similar to horse heart MbCO, which does not possess Arg45 (*27*). This similarity is difficult to understand if the salt bridge breaking between Arg45 of SW-MbCO and 6-propionate side change causes a dominant volume change.

Although the difference in ΔV_{Mb} between (WT and H64Q) and (H64L and H64V) can be explained by the polarity of the electrostatic interaction, ΔV_{Mb} for WT is about 8 cm^3 mol^{-1} smaller than that for H64Q. This fact suggests the presence of another factor. A plausible origin, which may cause the volume change, is the entrance of the distal water into the distal pocket. The X-ray crystallographic data indicates the presence of a water molecule (distal water) for the WT-deoxyMb, whereas the distal pocket is vacant for the other mutants we studied (*33*). Considering that the initial volume change (ΔV_f) is negative only for WT-MbCO and positive for the other mutants (Figure 4a), one may reasonably speculate that one of the origins of the initial volume change is related with this distal water as described next. After the CO is photodissociated from the heme, the CO is transferred to the first trap site (*9*, *45*). The CO movement should cause the molecular volume expansion because it leaves an empty space in the protein. If a water molecule enters to the heme site as the exchange of the CO, the molecular volume of water compensates the space creation, and the molecular volume may not be changed. On the other hand, if a water molecule does not move to the heme site (this is a case for the other mutants), the movement of the CO causes a volume change. This mechanism explains the observed initial volume changes for WT and the other mutants. If this explanation is correct, the distal water should move into the heme site within a few nanoseconds after the CO escaping from the site, and this fast movement implies that this water molecule should be initially located inside the protein interior before the movement. The replacement of the heme site by the water may be accompanied by the random thermal motion of the water inside the protein interior. If we assume that the diffusion coefficient of CO in protein is not different so much from that in water ($D_{water} \sim 3 \times 10^{-9}$ m^2 s^{-1} (*25*)), the root-mean-square distance by the diffusion during 10 ps is 2.4 Å. This distance is probably long enough compared with the nearest distance between the heme pocket and a position where the water molecule was present.

In summary, we consider that the volume difference between MbCO and Mb is controlled by several factors: heme doming, the E and F helices movement, disappearance of the electrostatic interaction between CO and the polar distal residue, and movement of the distal water. If these are the all origins of the volume change, ΔV_{Mb} of H64L and H64V represents the volume change by the first two mechanisms (heme doming, the E and F helices movement). It should be noted that $-\Delta V_{Mb}$ is smaller than the partial molar volume of CO in solvents. Hence, we consider that some part of the heme space is reserved even after the CO escape from the space. The effect of the distal water movement may appear as the volume difference between WT and H64Q (volume contraction of about -5 cm^3 mol^{-1}). The contribution of the electrostatic interaction in the heme pocket explain the volume difference between (WT and H64Q) and (H64L and H64V) (about -10 cm^3 mol^{-1}).

5.2. Nature of CO Trapping Site. Next, to obtain an insight in the structure of the intermediate state, Mb:CO, we consider the volume change of Mb:CO from the final state (Mb), $\Delta V_{Mb:CO} = V(Mb:CO) - V(Mb) (= \Delta V_f - V_{Mb})$. Here we take the final Mb instead of the initial MbCO as the reference state because of the following reasons. First, we can neglect the effect of the salt bridge by taking the ligand-dissociated state as the reference because the salt bridge is broken for all of the myoglobins at this stage. Second, the effect of the electrostatic interaction between the distal residue and the bound ligand can be also neglected. Hence, we can minimize the effect of the mutation by this choice.

$\Delta V_{Mb:CO}$ can be regarded as the partial molar volume of CO inside the protein at the trapped site. $\Delta V_{Mb:CO}$ of the mutants we examined are depicted in Figure 4d. It is interesting to note that $\Delta V_{Mb:CO}$ for Mb with the nonpolar amino acid residues at the 64 position (H64L and H64V) are similar to each other (around $+33$ cm^3 mol^{-1}), and it is larger than those with the polar amino acid residues (WT and H64Q) (about $+25$ cm^3 mol^{-1}). The mutant dependent $\Delta V_{Mb:CO}$ may be explained by either two ways. First, it is possible that the CO trapped location is different depending on the amino acid residue at the 64 position. In this case, the route of the CO escaping process should be controlled by the distal residue. Second, although the CO trapping site is the same for the mutants and WT, the partial molar volume of the CO could be different. In general, a molecular volume is determined by the intermolecular interaction between the molecule and the matrix. The smaller partial molar volume of the CO for the Mb protein with the polar amino acid residue at the 64 position compared with that with the nonpolar amino acid residue suggests that the electrostatic interaction between the CO and the distal residue makes the CO volume smaller. If this is the case, the CO trapping site should be close to the distal position or, at least, the molecule at the position should be influenced by the distal residue.

It is also particularly interesting to note that $\Delta V_{Mb:CO}$ for Mb with the nonpolar amino acid residues is similar to the partial molar volume of CO in nonpolar solvent. This fact suggests that, first, the CO trapping process inside the protein is similar to the dissolution of CO in organic solvent; that is, the CO is surrounded by nonpolar amino acid residues tightly and, second, the CO should move into a position that was occupied by amino acid residues before the dissociation, but not into a vacant cavity. Frequently, the CO trapping site has been discussed with relation to two cavities (*46*, *47*)-observed by the X-ray crystallographic measurement (*48*, *49*). These cavities are located at the distal side and the proximal side of the heme, and they are known as Xe binding sites. The cavity of the distal side is called $Xe^{(4)}$ and that of

the proximal side is called $Xe^{(1)}$ (*50*). If the polarity of the residue 64 determines the environment of the CO trapping site, $Xe^{(1)}$ seems to be too far from residue 64. In contrast, $Xe^{(4)}$ is located near the residue 64 enough to affect the environment of the site. If these Xe sites are vacant cavities in the Mb interior, the results in this study may suggest that the Xe sites are not plausible locations for the CO trapping site. A recent study by Dantsker et al. showed that less photodissociated CO moves into the Xe sites in H64L-MbCO than in WT-MbCO. (*47*) Their study suggests that the difference in $\Delta V_{Mb:CO}$ could be attributed to the difference in the yield of CO entrance into the Xe sites. Although we need further research before the final conclusion whether $Xe^{(4)}$ and $Xe^{(1)}$ sites are relevant to the ligand storage sites or not, the information obtained in this work should be helpful in the understanding of the ligand escape process from the protein to the solvent.

5.3. Ligand Escape Rate. So far, a number of studies have been published on ligand recombination kinetics under a variety of conditions (such as temperatures, pressures, pH) for MbCO including various mutants (*2*, *3*, *18*, *19*, *22*). These studies revealed a complex barrier height distribution during the ligand recombination reaction. On the other hand, compared with the extensive studies on the recombination process, information on the ligand escaping process, which should be very important to seek the relationship between the protein dynamics and the biological function, has been very limited, only because this escaping process is very difficult to detect by a conventional spectroscopy that monitors the optical transition of the heme. Using the TG technique, we can now detect the escaping process in time-domain under various conditions. In the present study, we found that the escape rate from the protein interior depends on the site-directed mutation at the His64. When His64 is replaced by a nonpolar residue such as Leu or Val, the escape rate increases to around 400 ns. On the other hand, when it is replaced by a polar residue Q, the rate (850 ns) is similar to WT-MbCO (700 ns). Therefore, not only $\Delta V_{Mb:CO}$ but also the escape rate are controlled by the polarity of the residue 64. This result also suggests that the CO trapped site is different depending on the polarity of the residue 64 or the nature of the trapped site is sensitive to this polarity. In any case, the ligand escape process is controlled by the residue 64. This observation again questions the participation of $Xe^{(1)}$ site as the CO storage site. Studies on this rate under various conditions will be useful to elucidate the escape route of the ligand.

CONCLUSION

In this study, we investigated the origins of the volume change accompanied by the photodissociation process of MbCO by using the mutants in which His64 is replaced by Leu, Val, and Gln. We found that the volume change strongly depends on amino acid residue at position 64 in Mb. We considered the effect of the heme doming, the E and F helices movement, electrostatic interaction between the bound CO and the distal residue, and the movement of the distal water. We found that the main factor to determine the amplitude of the volume change is the polarity of the amino acid. Hence, we suggest that the polar residue at position 64 induces the volume contraction after the photodissociation of CO from the heme because of the disappearance of the repulsive electrostatic interaction between the bound CO and the polar residue 64. In contrast, such a contraction does not occur in the case of H64L- and H64V-MbCOs, since the apolar residue at the position 64 has a weak interaction with the bound CO. Although the difference in volume between Mb and MbCO comes from mainly the movement of E and F helices induced by the heme doming, the contraction effect due to the polarity of residue 64 makes the volume of Mb smaller for WT and H64Q. The volume difference between the intermediate (Mb:CO) and Mb ($\Delta V_{Mb:CO}$) gave information on the nature of the CO trap site. From the difference in ΔV_{MbCO} between four MbCOs, we conclude that the polarity of the residue 64 affects the nature of the CO trap site.

ACKNOWLEDGMENT

The authors are indebted to Dr. S. Takahashi, Prof. K. Ishimori, and K. Konishi of Kyoto University for fruitful discussions and instruction in preparation of the sample.

REFERENCES

1. Austin, R. H., Beeson, K. W., Eisenstein, L., Frauenfelder, H., and Gunsalus, I. C. (1975) *Biochemistry 14*, 5355−5373.
2. Springer, B. A., Sriger, S. G., Olson, J. S., and Phillips, G. N., Jr. (1994) *Chem. Rev. 94*, 699−714.
3. Olson, J. S., and Phillips, G. N., Jr. (1996) *J. Biol. Chem. 271*, 17593−17596.
4. Srajer, V., Reinishch, L., and Champion, P. M. (1988) *J. Am. Chem. Soc. 110*, 6656−6670.
5. Champion, P. M. (1992) *J. Raman. Spectrosc. 23*, 557−567.
6. Srajer, V., and Champion, P. M. (1991) *Biochemistry 30*, 1390−1402.
7. Takano, T. (1977) *J. Mol. Biol. 110*, 569−584.
8. Kuriyan, J., Wilz, S., Karplus, M., and Petsko, G. A. (1986) *J. Mol. Biol. 192*, 133−154.
9. Lim, M., Jackson, T. A., and Anfinrud, P. A. (1997) *Nat. Struct. Biol.* 209−214.
10. Cansgrove, T. P., and Dyer, R. B. (1996) *J. Phys. Chem. 100*, 3273−3277.
11. Xie, X., and Simon, J. D. (1991) *Biochemistry 30*, 3682−3692.
12. Sakan, Y., Ogura, T., Kitagawa, T., Fraunfelter, F. A., Mattera, R., and Ikeda-Saito, M. (1993) *Biochemistry 32*, 5815−5824.
13. Nukashima, S., Kitagawa, T., and Olson, J. S. (1998) *Chem. Phys. 228*, 323−336.
14. Mukai, M., Nakashima, S., Olson, J. S., and Kitagawa, T. (1998) *J. Phys. Chem. B. 102*, 3624−3630.
15. Martin, J. L., Migus, A., Poyart, C., Lecarpentier, Y., Astier, R., and Antonetti, A. (1983) *Proc. Natl. Acad. Sci. U.S.A. 80*, 173−177.
16. Franzen, S., Bohn, B., Poyart, C., and Lecarpentier, Y., Astier, R., and Antonetti, A. (1983) *Proc. Natl. Acad. Sci. U.S.A. 80*, 173−177.
17. Henry, E. R., Sommer, J. H., Hofrichter, J., and Eaton, W. A. (1983) *J. Mol. Biol. 166*, 443−451.
18. Carver, T. E., Rohlfs, R. J., Olson, J. S., Gibson, Q. H., Blackmore, R. S., Springer, B. A., and Sligar, S. G. (1990) *J. Biol. Chem. 265*, 20007−20020.
19. Lambright, D. G., Balasubramanian, S., Decatur, S. M., and Boxer, S. G. (1994) *Biochemistry 33*, 5518−5145.
20. Esquerra, R. M., Goldbeck, R. A., Kim-Shapiro, D. B., and Kliger, D. S. (1998) *Biochemistry 37*, 17527−17536.
21. Ansari, A., Jones, C. M., Henry, E. R., Hofrichter, J., and Eaton, W. A. (1994) *Biochemistry 33*, 5128−5145.
22. Ishikawa, H., Uchida, T., Takahashi, S., Ishimori, K., and Morishima, I. (2001) *Biophys. J. 80*, 1507−1517.
23. Kleinert, T., Doster, W., Leyser, H., Petry, W., Schwarz, V., and Settles, M. (1998) *Biochemistry 37*, 717−733.
24. Terazima, M. (1998) *J. Phys. Chem. A. 102*, 545−551.

25. Hara, T., Hirota, N., and Terazima, M. (1996) *J. Phys. Chem. 100*, 10194−10200.
26. Sakakura, M., Yamaguchi, S., Hirota, N., and Terazima, M. (2001) *J. Am. Chem. Soc. 123*, 4286−4294.
27. Sakakura, M., Morishima, I., and Terazima, M. (2001) *J. Phys. Chem. B. 105*, 10424−10434.
28. Dadusc, G., Ogilvie, J., Schulenberg, P., Marvet, U., and Miller, R. J. D. (2001) *Proc. Natl. Acad. Sci. U.S.A. 98*, 6110−6115.
29. Richard, L., Genberg, L., Deak, J., Chiu, H. L., and Miller, R. J. (1992) *Biochemistry 31*, 10703−10715.
30. Deak, J., Chiu, H. L., Lewis, C. M., and Miller, R. J. D. (1998) *J. Phys. Chem. B. 102*, 6621−6634.
31. Westrick, J. A., Peters, K. S., Ropp, J. D., and Sligar, S. G. (1990) *Biochemistry 29*, 6741−6746.
32. Borsarelli, C. D., and Braslavsky, S. E. (1998) *J. Phys. Chem. B. 102*, 6231−6238.
33. Quillin, M. L., Arduini, R. M., Olson, J. S., and Phillips, G. N., Jr. (1993) *J. Mol. Biol. 234*, 140−155.
34. Quillin, M. L., Li, T., Olson, J. S., Phillips, G. N., Jr., Dou, Y., Ileda-Saito, M., Regan, R., Carlson, M., Gibson, Q. H., Li, H., and Elber, P. (1995) *J. Mol. Biol. 245*, 416−436.
35. Ray, G. B., Li, X. Y., Ibers, J. A., Sessler, J. L., and Spiro, T. G. (1994) *J. Am. Chem. Soc. 116*, 162−176.
36. Li, T., Quillin, M. L., Phillips, G. N., Jr., and Olson, J. S. (1994) *Biochemistry 33*, 1433−1446.
37. Jewsbury, P., and Kitagawa, T. (1995) *Biophys. J. 68*, 1283−1294.
38. Eichler, H. J., Gunter, P., and Paul, D. W. (1986) *Laser-Induced Dynamic Gratings*, Springer-Verlag, Berlin.
39. Ukai, A., Hirota, N., and Terazima, M. (2000) *J. Phys. Chem. A. 104*, 6681−6688.
40. Ben-Amotz, D., and Harris, C. B. (1987) *J. Chem. Phys. 86*, 4856−4870.
41. Springer, B. A., and Sligar, S. G. (1987) *Proc. Natl. Acad. Sci. U.S.A. 84*, 8961−8965.
42. Sugimoto, T., Unno, M., Shiro, Y., Dou, Y., and Ikeda-Saito, M. (1998) *Biophys. J. 75*, 2188−2194.
43. Kachalova, G. S., Popov, A. N., and Bartunik, H. D. (1999) *Science 284*, 473−476.
44. Johnson, K. A., Olson, J. S., and Phillips, G. N., Jr. (1989) *J. Mol. Biol. 207*, 459−463.
45. Srajer, V., Teng, T., Ursby, T., Pradervand, C., Ren, Z., Adachi, S., Schildkamp, W., Bourgeois, D., Wulff, M., and Moffat, K. (1996) *Science 274*, 1726−1729.
46. Scott, E. E., Gibson, Q. H., and Olson, J. S. (2001) *J. Biol. Chem. 276*, 5177−5188.
47. Dantsker, D., Samuni, U., Friedman, A. J., Yang, M., Ray, A., and Friedmann, J. M. (2002) *J. Mol. Biol. 315*, 239−251.
48. Chu, K., Vojtchovsky, J., Mcmahon, B. H., Sweet, R. M., Berendzen, J., and Schlichting, I. (2000) *Nature 403*, 921−923.
49. Ostermann, A., Waschipky, R., Parak, F. G., and Nienhaus, G. U. (2000) *Nature 404*, 205−208.
50. Tilton, R. F., Jr., Kuntz, I. D., Jr., and Petsko, G. A. (1984) *Biochemistry 23*, 2849−2857.

BI016085D